Imaging the model through the wave equation

Esteban Díaz, Satyan Singh, Roel Snieder, and Paul Sava,
Center for Wave Phenomena, Colorado School of Mines

SUMMARY

Two-way wavefields generated with the Marchenko method are able to reproduce complex wave phenomena that includes primaries, internal multiples and surface-related multiples. The wavefield contains reflections and information from the true model, but propagating with the kinematics of an input background velocity model. We design an inverse problem to find a model that explains the scattering phenomena present in the reconstructed wavefield. The two-way nature of the Marchenko wavefields allows us to use them with the homogeneous wave equation and obtain images that are indicative of subsurface model parameters. Unlike conventional imaging methods, where the image is indicative of the interfaces in the subsurface, our method inverts for the properties within the subsurface. Our tests show that one can invert for images indicative of the true model even when the background velocity model is partially inaccurate. Furthermore, we are able to image properties from the true model that are not part of the inputs used to generate the wavefield.

INTRODUCTION

Seismic imaging methods aim to estimate the Earth's reflectivity, i.e., a map of the interfaces that scatter the propagating wavefields. However, a seismic image does not only have structural information, but also dynamic properties that contain important information about the subsurface parameters (Etgen et al., 2009). Despite great advances in seismic exploration technology, the underlying imaging mechanisms (the imaging condition) are essentially the same as the one proposed by Claerbout (1971).

The wavefield reconstruction step is where many advances occurred recently. The source and receiver wavefields can be extrapolated with integral formulations as in Kirchhoff migration (Schneider, 1978), one-way equations as in wave equation migration (WEM) (Gazdag, 1978; Gazdag and Sguazzero, 1984), or two-way equations as in reverse time migration (RTM) (Baysal et al., 1983; Whitmore, 1983; McMechan, 1983). The three outlined families have a basic assumption in common: the single-scattering (Born) approximation. Hence, the multiple-scattered waves present in the data are imaged in the wrong position. Therefore, the multiples are usually eliminated pre imaging (Verschuur et al., 1992; Weglein et al., 1997; Guitton, 2005; Lin and Herrmann, 2013) or post imaging (Sava and Guitton, 2005; Wang et al., 2010; Weibull and Arntsen, 2013).

Marchenko imaging retrieves the Green's function and properly handles primaries and internal multiples given a background velocity model with the appropriate kinematics. The Marchenko modeling framework (Broggini and Snieder, 2012; Behura et al., 2014; Wapenaar et al., 2014; Singh et al., 2015a) solves for focusing functions that are used to retrieve the total Green's function, which can be decomposed into up- and down-going components. This framework is also applicable to surface-related multiples (Singh et al., 2015a,b). The total Green's function satisfies the acoustic wave equation with all the scattering present in the data.

In this paper, we use the total Green's function instead of the individual up- or down-going components (or source and receiver wavefields) to obtain an image of the model parameters (instead of the reflectivity). We use the total Green's functions together with relations given by the wave equation to obtain images sensitive to other subsurface properties like density or impedance.

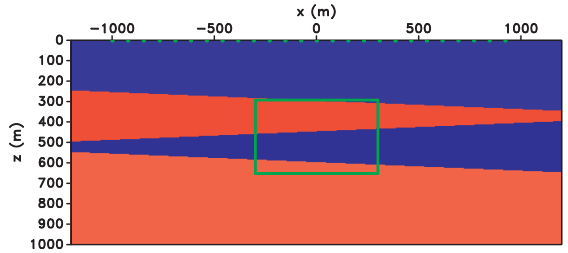

(a)

Figure 1: Variable velocity model: the points at the surface denote source locations and the highlighted box indicates the area in which the Marchenko wavefield is retrieved.

IMAGING THE MODEL PARAMETERS

The Marchenko framework outlined in Singh et al. (2015a) allows for the Green's function retrieval with pressure-normalized fields. The method reconstructs the Green's function from any point $\mathbf{x}$ inside the medium to the surface. The method requires the reflectivity response $R(\mathbf{x}_s, \mathbf{x}_r, t)$ for sources $\mathbf{x}_s$ and receivers $\mathbf{x}_r$ located at $z = 0$. It also requires an estimate of the transmission response $T_d(\mathbf{x}, \mathbf{x}_r, t)$ from the point of interest $\mathbf{x}$ to the surface. In practice, T_d is approximated by the first arrivals in the background medium, which can be obtained with either a finite difference approach or an eikonal traveltime data convolved with an appropriate wavelet.

From the data and the transmission response, the Marchenko

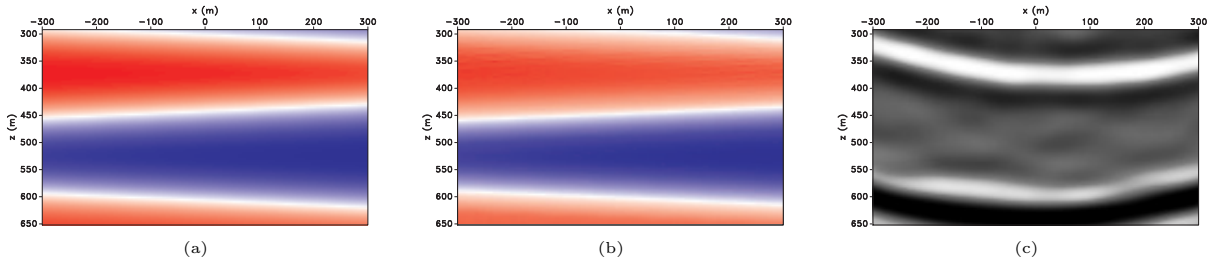

(a) (b) (c)

Figure 2: Velocity retrieval: (a) is a smooth background model used for computing the transmission response T_d, (b) the retrieved velocity model, and (c) a snapshot of the wavefield $u(\mathbf{x}, \mathbf{x}_s = (0,0), t = 0.6s)$. Note how the retrieved model converges to the background model.

framework retrieves the Green's function from all the points in the subsurface to the surface. The retrieved wavefield $u(\mathbf{x}, \mathbf{x}_s, t)$ satisfies the acoustic wave equation. If the transmission response is accurate enough, the wave equation is satisfied for the true model parameters.

We use the total wavefield u to retrieve model parameters, like density and velocity, present in the wave equation. The retrieved wavefields are used as an input to the wave equation from which we solve for specific model parameters. This idea have been successfully implemented in the medical community for finding elastic parameters of human tissues (Manduca et al., 2001). Here we show an inversion framework for acoustic parameters.

Constant velocity acoustics

Consider the constant density homogeneous wave equation

$$s^2 \frac{\partial^2 u}{\partial t^2} - \nabla^2 u = 0, \tag{1}$$

where $s^2(\mathbf{x})$ is the slowness squared and $u(\mathbf{x}_s, \mathbf{x}, t)$ the Marchenko wavefield generated from the source location $\mathbf{x}_s$. Note that the wavefield can be obtained inside the medium away from the source location $\mathbf{x}_s$ where the homogeneous equation is satisfied.

In order to solve for the unknown field $s^2(\mathbf{x})$, one can set up a least-squares linear problem:

$$J(s^2) = \left|\left| s^2 \frac{\partial^2 u}{\partial t^2} - \nabla^2 u \right|\right|_2^2, \tag{2}$$

which has the following solution:

$$s^2(\mathbf{x}) = \frac{\sum_{t,\mathbf{x}_s} \frac{\partial^2 u(\mathbf{x}_s,\mathbf{x},t)}{\partial t^2} \nabla^2 u(\mathbf{x}_s, \mathbf{x}, t)}{\sum_{t,\mathbf{x}_s} \left(\frac{\partial^2 u(\mathbf{x}_s,\mathbf{x},t)}{\partial t^2} \right)^2}. \tag{3}$$

Observe how this expression closely resembles the least squares solution for the deconvolution imaging condition (Claerbout, 1971; Guitton et al., 2007).

The kinematics embedded in the Marchenko wavefield u are driven by the first arrival information $T_d(\mathbf{x}_s, \mathbf{x}, t)$ which is computed using a background velocity model. The inversion procedure outlined in equation 2 utilizes the geometric attributes of the wavefield; therefore, the wave equation is satisfied for the same background velocity model used for computing the transmission response $T_d(\mathbf{x}_s, \mathbf{x}, t)$.

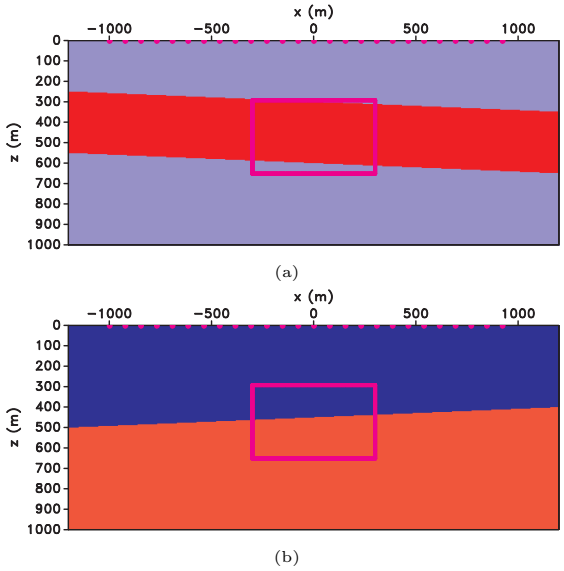

(a)

(b)

Figure 3: (a) Variable velocity and (b) density model. Note how the density and velocity model are decoupled inside the box.

Variable density acoustics

For variable density, the Marchenko wavefield u satisfies the wave-equation

$$\frac{s^2}{\rho} \frac{\partial^2 u}{\partial t^2} - \nabla \cdot \left(\frac{1}{\rho} \nabla u \right) = 0. \tag{4}$$

The relation of the wavefield $u(\mathbf{x}_s, \mathbf{x}, t)$ with the model parameters $s^2(\mathbf{x}_s, \mathbf{x}, t)$ and density $\rho(\mathbf{x})$ is not as trivial as in the previous case. This problem does not have a direct least squares solution. Considering that the kinematics are controlled by the model used as input to compute T_d, we can focus our attention on the density model ρ. Using only the homogeneous wave equation (for pressure), one cannot retrieve the magnitude of the density field because it scales all the terms in the equation. However, one should be able to retrieve the relative changes in the density field. As with the constant

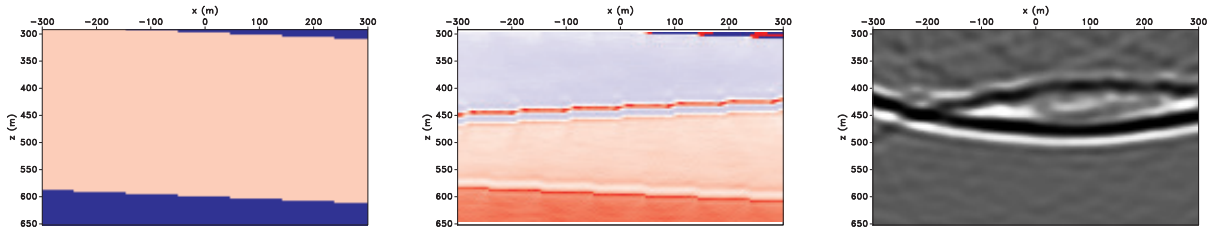

(a) (b) (c)

Figure 4: Density retrieval: (a) exact velocity model used as background, (b) inverted density model, and (c) a snapshot of the wavefield $u(\mathbf{x}, \mathbf{x}_s = (0,0), t = 0.6s)$. Note how the velocity layer leaks into the inverted model. However, the density layer and interface are clearly defined in the inverted model.

density case, we set the following optimization goal:

$$J\left(\frac{1}{\rho}\right) = \left|\left|\frac{s^2}{\rho}\frac{\partial^2 u}{\partial t^2} - \nabla\cdot\left(\frac{1}{\rho}\nabla u\right)\right|\right|_2^2. \quad (5)$$

Numerically, the problem is implemented as follows:

$$J(m) = ||\mathbf{D_t} m + \mathbf{D}\mathbf{G_u} m||_2^2 = ||L(m)||_2^2, \quad (6)$$

where $\mathbf{D_t} = diag\{s^2(\mathbf{x})\frac{\partial^2 u(\mathbf{x}_s,\mathbf{x},t)}{\partial t^2}\}$, $\mathbf{G_u}$ is a block diagonal matrix that contains the gradient of u, and $\mathbf{D}$ is the divergence matrix.

The gradient with respect to the buoyancy $m = 1/\rho$ is given by

$$\nabla_m J = \mathbf{D_t}^\top L(m) + \mathbf{G_u}^\top \mathbf{D}^\top L(m), \quad (7)$$

where $^\top$ denotes adjoint. Once the gradient is defined, the model is updated iteratively using a non-linear solver.

Pressure and particle velocity relations

Another option for retrieving an image of the buoyancy is to use the relations between pressure fields and particle velocity. The Marchenko framework described in Singh et al. (2015a, 2016) allows for the reconstruction of pressure u and the vertical component of the particle velocity v_z fields. Hence, we can find the model that best matches the acoustodynamics relation:

$$\frac{\partial V_z}{\partial t} = -\frac{1}{\rho}\frac{\partial u}{\partial z}. \quad (8)$$

Similarly to as in the first case, we can solve a linear least-squares problem to find the appropriate solution:

$$J(m) = \left|\left|\frac{\partial V_z}{\partial t} + m\frac{\partial u}{\partial z}\right|\right|_2^2, \quad (9)$$

which has a solution that resembles equation 3:

$$m = -\frac{\sum_{t,\mathbf{x}_s}\frac{\partial V_z}{\partial t}(\mathbf{x},\mathbf{x}_s,t)\frac{\partial u}{\partial z}(\mathbf{x},\mathbf{x}_s,t)}{\sum_{t,\mathbf{x}_s}\left(\frac{\partial u}{\partial z}(\mathbf{x},\mathbf{x}_s,t)\right)^2}. \quad (10)$$

We have presented two options to invert for parameters given the pressure wavefield (first two cases) or the pressure and particle velocity wavefields (last case). These approaches are not the only options; one could try to reparametrize the wave equation in terms of acoustic impedance or other suitable combinations.

EXAMPLES

We test the imaging procedure described above for two cases: constant and variable density. For each case, we test the sensitivity to the background velocity model and compute acoustic data with a free surface boundary condition. In order to record both pressure and particle velocity data, we use the finite difference implementation of the coupled acoustodynamics system of equations from Thorbecke and Draganov (2011).

We place 500 sources and receivers at $z = 0$m in the range $x = [-1000, +1000]$m (Figure 1) to generate data. The input transmission data $T_d(\mathbf{x}, \mathbf{x}_s, t)$ are computed using an eikonal solver.

Figure 1 shows the velocity model and the highlighted box depicts the area where the Marchenko wavefields are retrieved. The dots in the surface indicate the source locations used for the imaging process (a subset of the sources present in the data).

Figure 2a depicts a smooth version of the true velocity used as the background model. The Marchenko wavefields show propagating waves, with the corresponding reflections, even if the background velocity model is smooth (Figure 2c). One could say that the retrieved wavefield is an expression of the true Green's function with the kinematics of the background model. Figure 2b is the inverted velocity model using the same procedure as discussed above. Note that the inverted model converges to the background model. This is because the kinematics of the retrieved wavefield are given by the background model, but the reflections present in the wavefield are due to the discontinuities of the original model.

The model parameters for the variable density experiment are shown in Figures 3a-3b. The density and velocity model contain complementary structure to see how well the inverted model can decouple reflections from either parameter. Since the kinematics of the wavefield converge to those of the background model, we focus our attention on the independent parameter, which is density in this case. Figure 4a shows the background model inside the box (the true model), whereas Fig-

ure 4b shows the inverted density model. The velocity interfaces leak into the inverted model, but, the density layers and the interface are well-imaged. Note that the density model is not an input for the computation of the wavefield shown in Figure 4c and yet the inverted image clearly delineates the density layer. In this example, we use the relation between pressure and particle velocity fields (equation 10) to compute the density image.

Figure 5a shows a smooth version of the true model used as background velocity field, and Figure 5b depicts the inverted density model. The density layer is clearly imaged despite the smooth background velocity model. The velocity interfaces again leak into the inverted model; note that the background velocity model does not contain any interface and yet the velocity interfaces from the original (true) model are imaged. The wavefield snapshot in Figure 5c is propagated in the smooth background model and contains all the reflections from the true model. Figure 5d is a density inversion from the pressure field (equation 6). By only using the pressure field, there is ambiguity with the magnitude of the density model because many different density models can yield the same wavefield. The model is clearly imaged with this method as the density layers are visible and there is only a hint from the velocity interface leaking into the inverted model. This approach is a valid alternative when one only have the pressure data as input, instead of the pressure and particle velocity data needed for the previous variable density examples.

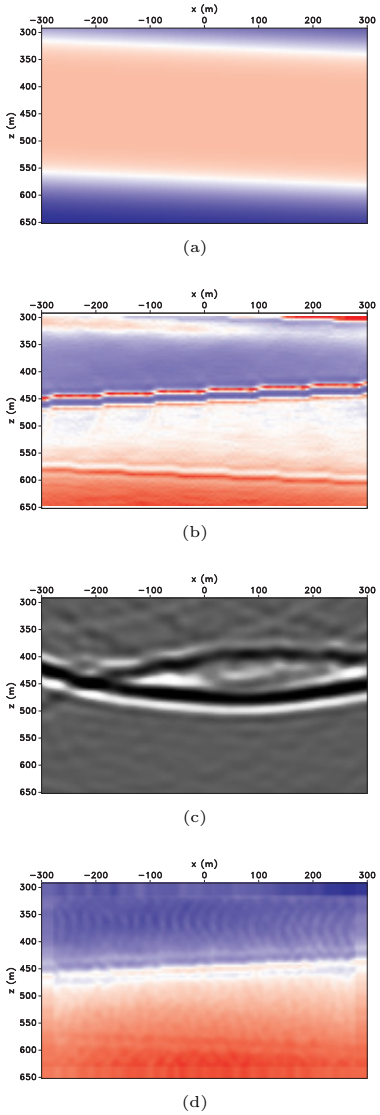

Figure 5: Density retrieval: (a) smooth velocity model used as background, (b) inverted density model from pressure and particle velocity data, (c) a snapshot of the wavefield $u(\mathbf{x}, \mathbf{x}_s = (0,0), t = 0.6s)$, and (d) density image from pressure only inversion. Note how the velocity layer leaks into the inverted model. However, the density layer and interface are clearly defined in the inverted models.

CONCLUSIONS

We present a framework to obtain images of acoustic model parameters that are different from reflectivity. Our method relies on two-way wavefields computed with Marchenko modeling. The wavefields are input into the wave equation together with the background velocity to find the model that explains, in a least-squares sense, the homogeneous wave equation. We show different options one could use depending on which type of data are available. One can exploit the relations between pressure and particle velocity and invert for the density model or one could use an iterative approach if pressure is the only available data. Our tests show that it is possible to find an image representing the true model even when the background model is smooth. This method is able to image the properties within the subsurface instead of the properties contrasts as it is done with conventional images.

ACKNOWLEDGMENTS

We thank the sponsors of the Center for Wave Phenomena, whose support made this research possible. The reproducible numeric examples in this paper use the Madagascar open-source software package (Fomel et al., 2013) freely available from http://www.ahay.org.

REFERENCES

Baysal, E., D. D. Kosloff, and J. W. C. Sherwood, 1983, Reverse time migration: Geophysics, **48**, 1514–1524.

Behura, J., K. Wapenaar, and R. Snieder, 2014, Autofocus imaging: Image reconstruction based on inverse scattering theory: Geophysics, **79**, A19–A26.

Broggini, F., and R. Snieder, 2012, Connection of scattering principles: a visual and mathematical tour: European Journal of Physics, **33**, 593.

Claerbout, J. F., 1971, Toward a unified theory of reflector mapping: Geophysics, **36**, 467–481.

Etgen, J., S. Gray, and Y. Zhang, 2009, An overview of depth imaging in exploration geophysics: Geophysics, **74**, WCA5–WCA17.

Fomel, S., P. Sava, I. Vlad, Y. Liu, and V. Bashkardin, 2013, Madagascar: open-source software project for multidimensional data analysis and reproducible computational experiments: Journal of Open Research Software, **1**, e8.

Gazdag, J., 1978, Wave equation migration with the phase-shift method: Geophysics, **43**, 1342–1351.

Gazdag, J., and P. Sguazzero, 1984, Migration of seismic data by phase shift plus interpolation: Geophysics, **49**, 124–131.

Guitton, A., 2005, Multiple attenuation in complex geology with a pattern-based approach: Geophysics, **70**, V97–V107.

Guitton, A., A. Valenciano, D. Bevc, and J. Claerbout, 2007, Smoothing imaging condition for shot-profile migration: Geophysics, **72**, S149–S154.

Lin, T. T. Y., and F. J. Herrmann, 2013, Robust estimation of primaries by sparse inversion via one-norm minimization: Geophysics, **78**, R133–R150.

Manduca, A., T. Oliphant, M. Dresner, J. Mahowald, S. Kruse, E. Amromin, J. Felmlee, J. Greenleaf, and R. Ehman, 2001, Magnetic resonance elastography: Non-invasive mapping of tissue elasticity: Medical Image Analysis, **5**, 237 – 254.

McMechan, G. A., 1983, Migration by extrapolation of time-dependent boundary values: Geophysical Prospecting, **31**, 413–420.

Sava, P., and A. Guitton, 2005, Multiple attenuation in the image space: Geophysics, **70**, V10–V20.

Schneider, W. A., 1978, Integral formulation for migration in two and three dimensions: Geophysics, **43**, 49–76.

Singh, S., R. Snieder, J. Behura, J. van der Neut, K. Wapenaar, and E. Slob, 2015a, Marchenko imaging: Imaging with primaries, internal multiples, and free-surface multiples: Geophysics, **80**, S165–S174.

Singh, S., R. Snieder, J. van der Neut, J. Thorbecke, E. Slob, and K. Wapenaar, 2015b, Incorporating free-surface multiples in marchenko imaging: SEG Technical Program Expanded Abstracts 2015, 4328–4333.

———, 2016, Accounting for free-surface multiples in marchenko imaging: submitted to Geophysics.

Thorbecke, J. W., and D. Draganov, 2011, Finite-difference modeling experiments for seismic interferometry: Geophysics, **76**, H1–H18.

Verschuur, D. J., A. J. Berkhout, and C. P. A. Wapenaar, 1992, Adaptive surfacerelated multiple elimination: Geophysics, **57**, 1166–1177.

Wang, B., C. Mason, M. Guo, J. Cai, S. Gajawada, and D. Epili, 2010, Interactive demultiple in the postmigration depth domain: 3436–3440.

Wapenaar, K., J. Thorbecke, J. van der Neut, F. Broggini, E. Slob, and R. Snieder, 2014, Marchenko imaging: Geophysics, **79**, WA39–WA57.

Weglein, A. B., F. A. Gasparotto, P. M. Carvalho, and R. H. Stolt, 1997, An inversescattering series method for attenuating multiples in seismic reflection data: Geophysics, **62**, 1975–1989.

Weibull, W., and B. Arntsen, 2013, Reverse time demigration using the extended imaging condition: SEG Technical Program Expanded Abstracts 2013, 4015–4020.

Whitmore, N. D., 1983, Iterative depth migration by backward time propagation: SEG Technical Program Expanded Abstracts, **2**, 382–385.